6. Castro, W. E., Digest of Ph.D. thesis, Univ. West Virginia, Morgantown (1966).
7. Crawford, H. R., and G. T. Pruitt, Rept no. DTMB-1, prepared for David Taylor Model Basin Hydromechanical Lab., Washington, D. C. (1965).
8. Denn, M. M., and J. J. Roisman, *AIChE J.*, **15**, 000 (1969).
9. Dodge, D. W., and A. B. Metzner, *ibid.*, **5**, 189 (1959).
10. Elata, C., and J. Tirosh, *Israel J. Tech.*, **3**, 1 (1965).
11. ———, and M. Poreh, *Rheol. Acta*, **5**, 148 (1966).
12. ———, J. Lehrer and A. Kahanovitz, *Israel J. Tech.*, **4**, 87 (1966).
13. Ernst, W. D., *AIChE J.*, **12**, 581 (1966); *Am. Inst. Aeron. Astronaut. J.*, **5**, 906 (1967).
14. Fabula, A. G., *Proc. 4th Intem. Congr. Rheol.*, 3, 455 (1965).
15. ——— "Proc 6th Naval Hydrodynamics Symposium, Office Naval Res., Washington, D.C.; Ph.D. Thesis Pennsylvania State Univ., University Park (1966).
16. Gadd, G. E., *Nature*, **206**, 463 (1965).
17. Granville, P. S., *Hydromechanics Lab. t. n. no. 61*, David Taylor Model Basin, Washington, D. C. (1966).
18. Giesekus, H., *Rheol. Acta*, **5**, 239 (1966).
19. Laufer, J., *Natl. Advisory Comm. Aeron.* Rept. 1174 (1954).
20. Lummus, J. L., J. E. Fox and D. B. Anderson, *Oil Gas J.* No. 12, 87 (1961).
21. Marshall, R. J., and A. B. Metzner, *Ind. Eng. Chem. Fundamentals* **6**, 393 (1967).
22. Meter, D. M., and R. B. Bird, *AIChE J.*, **10**, 881 (1964).
23. Metzner, A. B., and G. Astarita, *ibid.*, **13**, 550 (1967).
24. ———, and M. G. Park, *J. Fluid Mech.*, **20**, 291 (1964).
25. ———, and F. A. Seyer, "Proc. 6th Naval Hydrodynamics Symposium," Office Naval Res., Washington, D. C. (1966).
26. ———, E. A., Uebler, and C. F. Chan Man Fong, *AIChE J.*, to be published.
27. Metzner, A. B., J. L. White, and M. M. Denn, *ibid.*, **12**, 863 (1966); *Chem. Eng. Prog.*, **62**, 12, 81 (1966).
28. Meyer, W. A., *AIChE J.*, **12**, 522 (1966).
29. Millikan, C. B., "Proc. 5th Intern. Congr. Appl. Mech.", p. 386, John Wiley, New York (1939).
30. Oliver, D. R., *Can. J. Chem. Eng.*, **44**, 100 (1966).
31. Patterson, G. K., and Zakin, J. L., *AIChE J.*, **13**, 513 (1967).
32. Phillips, O. M., *J. Fluid Mech.*, **27**, 131 (1967).
33. Rotta, J., *Ing. Arch.*, **24**, 258 (1956).
34. Sandborn, V. A., *Natl. Advisory Comm. Aeron. TN 3266* (1955).
35. Savins, J. G., *Soc. Petrol. Eng. J.*, **4**, 203 (1964); *Rheol. Acta*. **6**, 323 (1967).
36. ———, *AIChE J.*, **11**, 673 (1965).
37. Schlichting, H., "Boundary Layer Theory," 4th Ed., McGraw-Hill, New York (1960).
38. Seyer, F. A., Ph.D. thesis, Univ. Delaware, Newark (1968).
39. Seyer, F. A., and A. B. Metzner, *Can. J. Chem. Eng.*, **45**, 121 (1967).
40. Shertzer, C. R., Ph.D. thesis, Univ. Delaware, Newark (1965).
41. Singh, K., Ph.D. thesis, Pennsylvania State Univ., University Park (1966).
42. Tomita, Y., *Bulletin Jap. Soc. Mech. Eng.*, **9**, 730 (1966).
43. Townsend, A. A., "The Structure of Turbulent Shear Flow," Cambridge Univ. Press, Cambridge (1966).
44. Virk, P. S., et al. *J. Fluid Mech.*, **30**, 305 (1967).
45. Wells, C. S., J. Harkness and W. A. Meyer, LTV Research Center Rept. No. 0-71000/6R-22, submitted for publication, (1966).
46. Wells, C. S., Jr., Am. Inst. Aeron. Astronaut, J. **3**, 1801 (1965).
47. ———, and J. G. Spangler, *Phys. Fluids*, **10**, 1890 (1967).
48. White, J. L., and A. B. Metzner, *J. Appl. Polymer Sci.*, **7**, 1863 (1963).

Manuscript received Dec. 4, 1967. Revision received March 28, 1968; paper accepted April 14, 1968.

Mutually Dependent Heat and Mass Transfer in Laminar Duct Flow

E. M. SPARROW
University of Minnesota, Minneapolis, Minnesota

and T. S. CHEN
University of Missouri, Rolla, Missouri

An analysis is performed of the strongly coupled heat and mass transfer processes which result from sublimation of mass from the walls of a duct into a flowing gas, the latent heat being provided solely by convective transfer from the gas. The flow is assumed to be laminar and hydrodynamically developed. Results are given for the streamward variations of the bulk and wall temperatures and mass fractions, of the heat and mass transfer rates, and of the local heat transfer coefficient. Representative temperature and mass fraction profiles are also presented. Entrance lengths characterizing the near approach to fully developed conditions are tabulated. Comparisons are made of the present results (based on a parabolic velocity profile) with those based on a slug flow velocity profile. A subsidiary analysis using the Lévêque model is also performed and the results compared with those of the principal solution.

Heat transfer processes in duct and tube flows have been the subject of extensive analytical investigation for many years (*1*). In recent years, mass transfer processes in internal flows have also been studied analytically [for

example, (2, 3)]. However, relatively little consideration has been given to internal flow problems in which heat and mass transfer processes act simultaneously and are so strongly coupled that the heat transfer rate is controlled by the mass transfer rate, and vice versa. The present research is concerned with such coupled transport processes.

Consideration is given to a parallel-plate channel whose walls are coated with a sublimable material. The walls are thermally isolated from the external environment. The gas flow entering the channel may contain the vapor of the sublimable material, but with a concentration below the saturation value. Under these conditions, sublimation will occur at the duct walls, the latent heat of sublimation being supplied by means of convective transport from the flowing gas to the walls. The rates of heat and mass transfer are thus mutually dependent. The concentration of the vapor will increase in the streamward direction, while the temperature will decrease. At sufficiently large downstream distances, the concentration and temperature approach cross sectionally uniform, fully developed values.

The velocity field is assumed to be laminar and hydrodynamically developed at the duct inlet, while the temperature and vapor concentration are uniform over the entrance cross section.

The analysis of the just described problem involves the simultaneous solution of the energy and diffusion equations, with coupling provided by the boundary conditions. The energy and diffusion equations are found to share a common set of eigenvalues, but have different eigenfunctions.

Numerical results are obtained and presented for the streamward variations of the bulk temperature and concentration, of the wall temperature and concentration, of the local fluxes of heat and mass, and of the heat transfer coefficient. The length of the development region is deduced from the bulk temperature and concentration results. Representative temperature and concentration profiles are also presented.

As a reasonable point of departure, the case of a slug flow velocity profile has already been investigated (4). The slug flow solution was undertaken to provide general trends and to facilitate the resolution of various points of difficulty. In addition, a linearized vapor pressure-temperature relationship for the vapor-solid saturation condition was proposed and tested. Representative results from the slug flow solution will be compared with corresponding results for the more realistic parabolic velocity profile utilized in the present investigation.

ANALYSIS

Formulation

The logical starting point of the analysis is the conservation equations for the various transferred quantities. These equations may be significantly simplified by taking cognizance of the findings of the Appendix, where it is demonstrated that the change in the mass rate of flow between the entrance section and the fully developed region may be on the order of a few per cent. In addition, it is estimated (4) that, on the average, the transverse velocity at the duct wall is about 0.01% of the mean flow velocity. In light of this, it appears reasonable to neglect changes in the velocity profile as well as to delete the transverse velocity from the conservation equations. Thus, the velocity distribution is expressible as $u/U = (3/2)[1 - (y/h)^2]$, where y and h respectively represent the transverse coordinate* and the channel half height. It is also reasonable to regard the fluid properties as constant.

The pertinent equations are energy conservation and mass conservation, the latter applied to the vapor.

$$\frac{3}{2}U\left(1-\frac{y^2}{h^2}\right)\frac{\partial T}{\partial x}=\alpha\frac{\partial^2 T}{\partial y^2},$$

$$\frac{3}{2}U\left(1-\frac{y^2}{h^2}\right)\frac{\partial C}{\partial x}=D\frac{\partial^2 C}{\partial y^2} \qquad (1)$$

in which C represents the mass fraction of the vapor, and x is the axial coordinate measuring distances downstream from the entrance section.

It is convenient to recast the foregoing equations in dimensionless form by employing the definitions

$$\eta=\frac{y}{h},\quad \xi=\frac{x/h}{Uh/\alpha},\quad \theta=\frac{T-T_f}{T_o-T_f},\quad \phi=\frac{C-C_f}{C_o-C_f} \qquad (2)$$

where C_o and C_f represent the vapor mass fractions at inlet and in the fully developed region, and T_o and T_f are the inlet and fully developed temperatures. The denominator of the dimensionless coordinate ξ is the Peclet number. In terms of the new variables, the conservation equations become

$$\frac{3}{2}(1-\eta^2)\frac{\partial\theta}{\partial\xi}=\frac{\partial^2\theta}{\partial\eta^2},\quad \frac{3}{2}N_L(1-\eta^2)\frac{\partial\phi}{\partial\xi}=\frac{\partial^2\phi}{\partial\eta^2} \qquad (3)$$

The symbol N_L denotes the Lewis number α/D.

The boundary conditions will now be discussed. Owing to symmetry with respect to $y = 0$, consideration need only be given to one of the bounding walls, say $y = h$ (that is, $\eta = 1$). Since the wall is thermally isolated from the external environment, it is necessary that the heat transferred from the fluid to the wall be equal to the energy requirements of the sublimation process. As demonstrated elsewhere (4), the mathematical formulation of this energy balance yields†

$$\rho D\lambda_s\frac{\partial C}{\partial y}=-k\frac{\partial T}{\partial y} \quad \text{or}$$

$$\frac{\partial\phi}{\partial\eta}=N_L\left[\frac{c_p}{\lambda_s}\left(\frac{T_o-T_f}{C_f-C_o}\right)\right]\frac{\partial\theta}{\partial\eta} \qquad (4)$$

Within the framework of the analysis, the bracketed quantity appearing in Equation (4) is unity. To demonstrate this, each of Equations (1) is integrated across the duct cross section and along the duct length from the entrance ($x = 0$) to some location x^* in the fully developed region. Inasmuch as the temperature and mass fraction are uniform at both $x = 0$ and x^* (T_o, C_o and T_f, C_f respectively), there results

$$\dot{M}c_p(T_f-T_o)=2\int_o^{x^*}k\left(\frac{\partial T}{\partial y}\right)_h dx,$$

$$\dot{M}(C_f-C_o)=2\int_o^{x^*}\rho D\left(\frac{\partial C}{\partial y}\right)_h dx \qquad (5)$$

where $\dot{M}$ is the mass rate of flow. The right-hand sides of these equations are readily related through the first of Equations (4), so that

$$(T_o-T_f)=(\lambda_s/c_p)(C_f-C_o) \qquad (6)$$

Upon using Equation (6), the boundary condition (4) becomes

$$\frac{\partial\phi}{\partial\eta}=N_L\frac{\partial\theta}{\partial\eta} \quad \text{at} \quad \eta=1 \qquad (4a)$$

* $y = 0$ coincides with the duct centerline.

† In general, the local sublimation rate at the wall contains contributions from both diffusion and convection (5). However, in most sublimation processes, the latter is much smaller than the former.

Another boundary condition follows from the fact that each location on the wall is a solid-vapor saturation state, so that there is a unique relationship between the local vapor pressure and temperature at the wall. At a given total pressure, this condition can be expressed as $C_w = f(T_w)$, where f is a known function. The accommodation of a completely general saturation state relation would require that the governing equations of the problem be solved by finite-differences. To achieve an analytical solution, it is necessary to maintain the linearity of the problem, and to this end the following linearized saturation-state relation is introduced

$$C = aT + b \tag{7}$$

A method of finding the constants a and b from given thermodynamic data is described in the Appendix of reference 4 where, in addition, numerical tests of the utility of Equation (7) are carried out. It is concluded on the basis of these tests that Equation (7), taken together with the proposed procedure for finding a and b, is a satisfactory representation for the saturation state relation. When Equation (7) is applied at the wall and use is made of Equations (2) and (6), there follows

$$\phi = -(a\lambda_s/c_p)\theta \quad \text{at} \quad \eta = 1 \tag{8}$$

The other conditions that must be satisfied are symmetry at the duct centerline and profile uniformity at the entrance section. In terms of the variables of the analysis, these are

$$\frac{\partial\theta}{\partial\eta} = \frac{\partial\phi}{\partial\eta} = 0 \quad \text{at} \quad \eta = 0 \tag{9}$$

$$\theta = \phi = 1 \quad \text{at} \quad \xi = 0 \tag{10}$$

The problem that must now be solved consists of the conservation Equations (3) subject to the boundary and inlet conditions (4a), (8), (9), and (10).

Solution

Elemental solutions for Equations (3) may be written as

$$\theta(\xi,\eta) = Ae^{-\beta^2\xi}\Theta(\eta), \quad \phi(\xi,\eta) = Be^{-\gamma^2\xi}\Phi(\eta) \tag{11}$$

where the Θ and Φ functions obey

$$\Theta'' + \frac{3}{2}\beta^2(1-\eta^2)\Theta = 0,$$

$$\Phi'' + \frac{3}{2}N_L\gamma^2(1-\eta^2)\Phi = 0 \tag{12}$$

By imposing the wall boundary conditions (4a) and (8), one finds that

$$\beta = \gamma \tag{13}$$

and, additionally

$$\frac{B}{A} = -\left(\frac{a\lambda_s}{c_p}\right)\frac{\Theta(1)}{\Phi(1)}, \quad \frac{B}{A} = N_L\frac{\Theta'(1)}{\Phi'(1)} \tag{14}$$

or

$$-\left(\frac{a\lambda_s}{c_p}\right)\frac{\Theta(1)}{\Phi(1)} = N_L\frac{\Theta'(1)}{\Phi'(1)} \tag{14a}$$

The determination of Θ and Φ involves the solution of the homogeneous mathematical system (12) and (14a). This system is quite different from that typically encountered in entrance region heat transfer or mass transfer problems in that two differential equations contribute to the eigenvalue problem.

For fixed values of the physical parameters N_L and $a\lambda_s/c_p$, the Θ and Φ functions depend parametrically on β. Thus, one can define

$$F(\beta) = \left(\frac{a\lambda_s}{c_p}\right)\frac{\Theta(1)}{\Phi(1)} + N_L\frac{\Theta'(1)}{\Phi'(1)} \tag{15}$$

When $F(\beta) = 0$, the boundary condition (14a) is satisfied and β is an eigenvalue.

The successive eigenvalues for fixed values of N_L and $a\lambda_s/c_p$ were determined by systematically varying β so as to satisfy the condition $F(\beta) = 0$. The $\Theta(1)$, $\Theta'(1)$, $\Phi(1)$, and $\Phi'(1)$ values needed in the evaluation of $F(\beta)$ were obtained by numerical (Runge-Kutta) integration of Equations (12). The numerical integrations were performed with $\eta = 0$ as a starting point and with $\Theta'(0) = \Phi'(0) = 0$ and $\Theta(0) = \Phi(0) = 1$ as starting values.† A stepsize study revealed that $\Delta\eta = 0.01$ was sufficient for all of the cases investigated. Between 30 and 45 eigenvalues were determined for each case, depending on the requirements of subsequent series summations. The eigenfunctions corresponding to each eigenvalue follow directly from the numerical solutions of Equations (12). The numerical values of the eigenvalues are available upon request.

Owing to the linearity of the problem, the most general solution corresponding to fixed values of the parameters is obtained by summing over all eigenvalues, that is

$$\theta = \sum_{n=1}^{\infty} A_n e^{-\beta_n^2\xi}\Theta_n(\eta), \quad \phi = \sum_{n=1}^{\infty} B_n e^{-\beta_n^2\xi}\Phi_n(\eta) \tag{16}$$

It still remains to determine the series coefficients A_n and B_n, and the duct inlet conditions (10) are available for this purpose. Thus,

$$1 = \sum_{n=1}^{\infty} A_n\Theta_n(\eta), \quad 1 = \sum_{n=1}^{\infty} B_n\Phi_n(\eta) \tag{17}$$

In the process of finding series coefficients from equations such as (17), it is highly desirable to make use of an orthogonality relationship. For conventional entrance region problems the Sturm-Liouville theory provides the needed orthogonality condition. However, the mathematical system defined by Equations (12) and (14a) does not fall within the framework of the conventional Sturm-Liouville system, and it is therefore necessary to derive a special orthogonality condition. By a procedure similar to that of reference 4, one finds

$$\int_0^1 (1-\eta^2)[A_iA_j\Theta_i\Theta_j + (c_p/a\lambda_s)B_iB_j\Phi_i\Phi_j]d\eta = 0 \tag{18}$$

Now, one can return to the task of finding the coefficients A_n and B_n. Keeping the orthogonality condition of Equation (18) in mind, one multiplies the first of Equations (17) by $(1-\eta^2)A_m\Theta_m$ and the second of Equations (17) by $(1-\eta^2)(c_p/a\lambda_s)B_m\Phi_m$, adds the thus multiplied equations, and then integrates over the range from $\eta = 0$ to $\eta = 1$. After making use of the orthogonality condition and eliminating B_n by employing the first of Equations (14), there results

$$A_n = \frac{-\Theta_n'(1)\left(1 + \dfrac{c_p}{a\lambda_s}\right)}{\beta_n^2\displaystyle\int_0^1 \frac{3}{2}(1-\eta^2)\left[\Theta_n^2 + \left(\frac{a\lambda_s}{c_p}\right)\left[\frac{\Theta_n(1)}{\Phi_n(1)}\right]^2\Phi_n^2\right]d\eta} \tag{19}$$

† Owing to the homogeneity of the system, the arbitrary specification of $\Theta(0)$ and $\Phi(0)$ does not affect the magnitude of the eigenvalues.

For Equation (19), the distributions $\Theta(\eta)$ and $\Phi(\eta)$ as well as the boundary values of Θ and Φ and their derivatives are provided by the numerical solutions of Equations (12). The integration appearing in the denominator of Equation (19) was performed numerically as part of the same computer program which furnished the Θ and Φ solutions. Once A_n has been evaluated, then B_n follows from either of Equations (14).

With the A_n and B_n known, then the temperature and mass fraction functions θ and ϕ, Equations (16), are completely determined.

Application of Solutions

Numerical evaluation of Equations (16) provides the temperature and mass fraction at any point in the duct. The quantities T_f and C_f, which respectively appear in the dimensionless temperature and mass fraction variables, are found by solving Equation (6) in conjunction with a saturation state relation.§ From Equations (16), by introducing $\eta = 1$ and varying ξ, one can calculate the variation of the wall temperature and mass fraction along the length of the duct. The longitudinal distributions of bulk temperature and bulk mass fraction are also of interest. These quantities are defined as

$$T_b = \frac{\int_o^h u\ T\ dy}{\int_o^h u\ dy}, \quad C_b = \frac{\int_o^h u\ C\ dy}{\int_o^h u\ dy} \tag{20}$$

After introducing the variables of the analysis and using Equations (12), there is obtained

$$\frac{T_b - T_f}{T_o - T_f} = \frac{C_b - C_f}{C_o - C_f} = -\sum_{n=1}^{\infty} \frac{A_n}{\beta_n^2}\, e^{-\beta_n^2 \xi} \Theta_n'(1) \tag{21}$$

Another quantity of interest is the local heat flux rate at the wall. By employing Fourier's law in conjunction with the temperature solution (16), there is obtained

$$\frac{qh}{k(T_o - T_f)} = -\sum_{n=1}^{\infty} A_n\, e^{-\beta_n^2 \xi} \Theta_n'(1) \tag{22}$$

Closely related to the local wall heat flux is the local sublimation rate $\dot{m}$. In particular, $\dot{m} = q/\lambda_s$ or, in dimensionless terms,

$$\frac{\dot{m}h}{\rho D N_L (C_f - C_o)} = \frac{qh}{k(T_o - T_f)} \tag{23}$$

A local heat transfer coefficient $q/(T_b - T_w)$ can be evaluated in terms of quantities that have already been discussed. Thus,

$$N_{Nuh} = \left(\frac{q}{T_b - T_w}\right)\frac{h}{k} = \frac{\dfrac{qh}{k(T_o - T_f)}}{\left(\dfrac{T_b - T_f}{T_o - T_f}\right) - \left(\dfrac{T_w - T_f}{T_o - T_f}\right)} \tag{24}$$

in which N_{Nuh} is the local Nusselt number based on the channel half height h. At large values of x, the Nusselt number approaches a fully developed value given by

$$N_{Nuh} = \frac{\beta_1^2}{1 + [\Theta_1(1)/\Theta_1'(1)]\beta_1^2} \tag{24a}$$

§ The fully developed state (T_f, C_f) is a saturation state.

Numerical results for the foregoing quantities, as well as for other quantities of interest, will be presented and discussed in the next section.

RESULTS AND DISCUSSION

The numerical results depend parametrically on two dimensionless groups, the Lewis number N_L and $a\lambda_s/c_p$. The Lewis number was assigned values of 0.81, 2.0, and 3.5 which, among other gas mixtures, covers a wide range of gases and vapors in dilute binary solution with air (6). For $a\lambda_s/c_p$, values of 0.1, 1, and 10 were selected on the basis of property evaluations for air-water and air-naphthalene mixtures. Thus, a total of nine cases were considered for the numerical evaluations. The eigenvalues for these cases are omitted here in order to conserve space, but are available from the authors.

Bulk Temperature and Mass Fraction

Longitudinal distributions of bulk temperature and bulk mass fraction are presented in Figure 1. In terms of the dimensionless ordinate variables, the distributions of the bulk temperature and bulk mass fraction are identical [Equation (21)]. The abscissa represents the dimensionless distance from the entrance, with the denominator Uh/D representing the Peclet number for diffusion.|| The curves are drawn as solid, dot-dashed, and dashed lines, respectively for $N_L = 0.81$, 2.0, and 3.5. For each N_L, there are curves for $a\lambda_s/c_p = 0.1$, 1, and 10. To preserve clarity, the results for $N_L = 2.0$ are referred to the upper abscissa.

All curves decrease with increasing downstream distance. Since $T_o > T_f$, it follows that T_b decreases along the duct. On the other hand, $C_o < C_f$, and C_b increases with x. These findings are consistent with physical reasoning. The curves decrease rapidly at small x, with increasingly slower rates of change in evidence at larger x values. This reflects the fact that the rates of heat and mass transfer are greatest in the immediate neighborhood of the inlet and decrease with increasing downstream distance.

For N_L near unity (that is, 0.81), the results are relatively insensitive to $a\lambda_s/c_p$. On the other hand, as N_L departs more and more from unity, the results become increasingly sensitive to $a\lambda_s/c_p$. When $N_L < 1$, the curves are arranged in ascending order with $a\lambda_s/c_p$; the opposite ordering is in evidence for $N_L > 1$. At a given N_L, the transport processes appear to be more rapid with decreasing $a\lambda_s/c_p$ for $N_L < 1$ and to be more rapid with increasing $a\lambda_s/c_p$ when $N_L > 1$. These remarks about relative arrangement and relative development rates are relevant only for common values of Uh/D.

The numerical results for the bulk mass fraction C_b facilitate the computation of the rate of sublimation from any axial length of duct. Specifically, by integrating the second of Equations (1) across the section and along the length, it is seen that the rate of sublimation from both walls in the region between $x = 0$ and $x = x$ is $\dot{M}(C_b - C_o)$, where C_b is the bulk mass fraction at x. It therefore follows that the sublimation rate in a length of duct situated between x_i and x_j is $\dot{M}(C_{bj} - C_{bi})$, in which C_{bj} and C_{bi} are, respectively, the bulk mass fractions at x_j and x_i.

Comparisons between the present results and those for slug flow (4) will be made later.

Entrance Lengths

The bulk temperature and bulk mass fraction results can

|| In constructing the figure, it was found that the use of Uh/D gave a somewhat more compact presentation than does Uh/α, which appears in the ξ variable.

be employed to determine the entrance length. Typically, the entrance length is defined in terms of the approach of some physically important quantity to within a preassigned percentage of its fully developed value. In this investigation, the entrance length is defined as the condition corresponding to

$$\frac{T_b - T_f}{T_o - T_f} = \frac{C_b - C_f}{C_o - C_f} = 0.05 \qquad (25)$$

The results thus obtained are listed in Table 1, where, for purposes of comparison, the entrance lengths for slug flow (4) are also given.

Table 1. Entrance Lengths and Fully Developed Nusselt Numbers

		Entrance Length, $(x/h)/(Uh/D)$		
N_L	$a\lambda_s/c_p$	Parabolic flow	Slug flow (4)	N_{Nuh}
0.81	0.1	1.57	1.15	1.846
0.81	1.0	1.72	1.26	1.866
0.81	10.0	1.87	1.37	1.882
2.0	0.1	1.47	1.08	1.971
2.0	1.0	1.16	0.858	1.947
2.0	10.0	0.843	0.620	1.902
3.5	0.1	1.44	1.06	2.008
3.5	1.0	1.01	0.751	1.987
3.5	10.0	0.550	0.406	1.926

From the table, it is seen that the values of $(x/h)/(Uh/D)$ corresponding to the entrance length are on the order of unity. When the hydraulic diameter d_h $(= 4h)$ is used as the characteristic dimension instead of the half-height h, then the dimensionless entrance lengths $(x/d_h)/(Ud_h/D)$ range from about 0.1 to 0.03. Entrance lengths for laminar heat transfer and mass transfer in ducts typically lie in this range.

Inspection of the table reveals that the dimensionless entrance length is relatively insensitive to $a\lambda_s/c_p$ when N_L is near unity, but is increasingly sensitive to $a\lambda_s/c_p$ when N_L departs more and more from unity. Also, the dimensionless entrance length is a very weak function of N_L for small $a\lambda_s/c_p$, but is quite sensitive to N_L at larger values of $a\lambda_s/c_p$.

The entrance lengths for slug flow (4) are about 74% of those for parabolic flow, the relationship between the two sets of results being remarkably constant over the entire range of parameters that was investigated. The more rapid development experienced by the slug flow is physically reasonable.

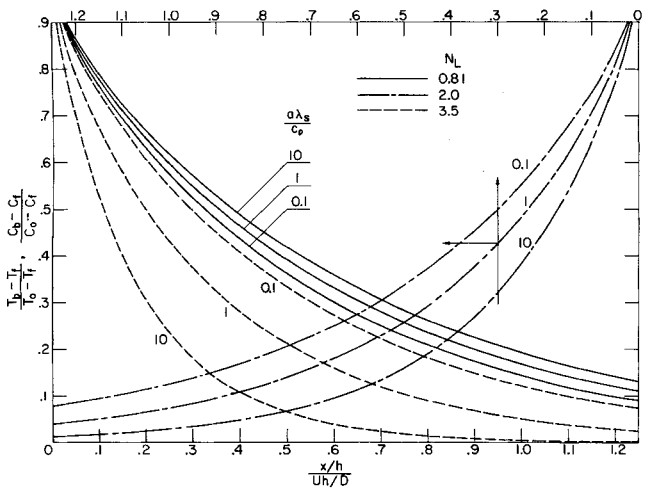

Fig. 1. Bulk temperature and bulk mass fraction distributions.

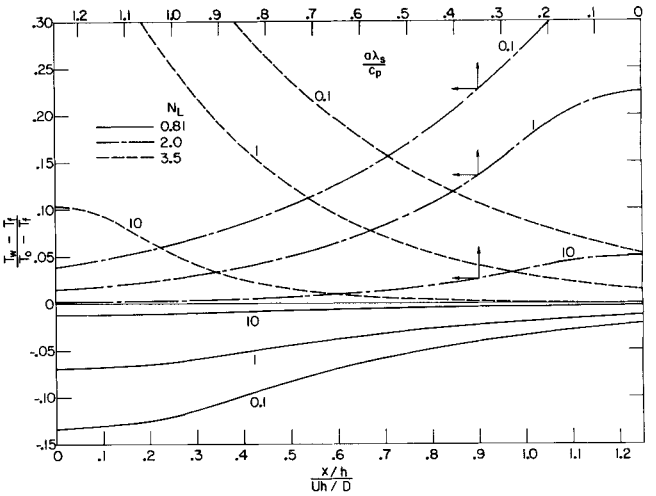

Fig. 2. Wall temperature distributions.

Wall Temperature and Mass Fraction

A graphical presentation of the variation of the wall temperature with distance along the duct is made in Figure 2. The structure of the figure and the parameterization of the curves is similar to that of Figure 1. In view of Equation (8), that is

$$\frac{C_w - C_f}{C_o - C_f} = -\left(\frac{a\lambda_s}{c_p}\right)\frac{T_w - T_f}{T_o - T_f} \qquad (26)$$

there is no need of a separate presentation of the results for the wall mass fraction.

Inspection of the figure reveals different trends depending upon whether $N_L < 1$ or $N_L > 1$. When $N_L < 1$, the wall temperature is always less than T_f, taking on its minimum value at $x = 0$ and increasing with increasing downstream distance along the duct. On the other hand, when $N_L > 1$, T_w always exceeds T_f; the maximum value of T_w occurs at $x = 0$, with steadily decreasing values in evidence as x increases.

With decreasing $a\lambda_s/c_p$ for $N_L > 1$, the values of T_w at $x = 0$ tend to approach more closely to T_o; correspondingly, the curves are arranged in ascending order according to decreasing $a\lambda_s/c_p$. Opposite trends are in evidence for $N_L < 1$.

The wall temperature distributions will be compared with those for the slug flow case in a later section.

Rates of Heat and Mass Transfer

The longitudinal distributions of the local wall heat and mass fluxes are presented in dimensionless form in Figure 3. In all cases, the heat and mass transfer rates take on very high values in the immediate neighborhood of the duct inlet. With increasing downstream distances, the rates of transfer decrease monotonically, asymptotically approaching zero.

In terms of the dimensionless variables of the figure, it appears that higher rates of transfer are associated with smaller values of N_L. However, care must be exercised in drawing such a conclusion. For instance, the dimensionless heat transfer group contains the quantity $(T_o - T_f)$, which is not independently prescribable, but is determined, for prescribed T_o and C_o, by solving Equation (6) in conjunction with a saturation state relation.

Heat Transfer Coefficients

The local Nusselt number, defined in Equation (24), provides a dimensionless representation of the local heat transfer coefficient. Figure 4 shows the longitudinal variation of the local Nusselt number. Aside from the immediate neighborhood of the entrance section, where very high values are achieved, the Nusselt number curves vary

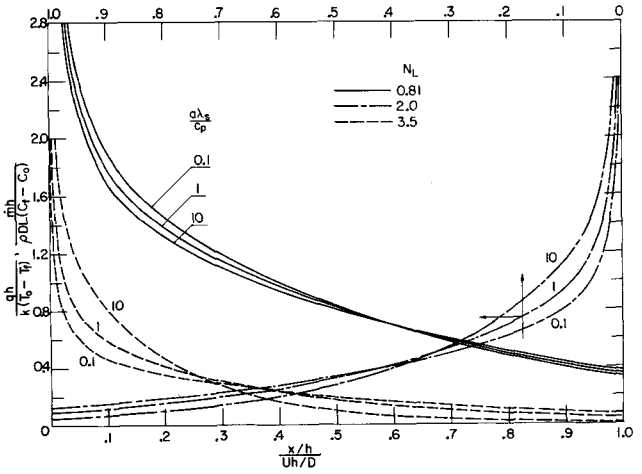

Fig. 3. Wall heat and mass flux distributions.

only slightly with increasing downstream distance. This behavior is in contrast to Figures 1, 2, and 3, where, in most cases, T_b, T_w, and q display substantial longitudinal variations in the same region in which the Nusselt number is more or less, unchanging. The relative constancy of the Nusselt number is not of direct utility in the present problem, since both q and $(T_b - T_w)$ are varying with position along the duct and neither is known *a priori*. Further inspection of Figure 4 shows that away from the entrance section, the Nusselt number results are relatively insensitive to the parameters N_L and $a\lambda_s/c_p$.

The details of the Nusselt number variations are somewhat unusual. For conventional thermal boundary conditions such as uniform wall temperature or uniform wall heat flux, the Nusselt number decreases monotonically, approaching the fully developed limit from above. On the other hand, Figure 4 shows that in some cases the Nusselt number attains a minimum value and then approaches the fully developed limit from below. There does not appear to be an intuitively simple explanation for this behavior.

It is interesting to compare the fully developed Nusselt numbers, Equation (24*a*), with those for the limiting cases of uniform wall temperature and uniform heat flux, respectively 1.885 and 2.059. The results for the present problem are listed in Table 1. It is seen that the Nusselt numbers for $N_L = 0.81$ are lower than that for uniform wall temperature (that is, < 1.885), while those for $N_L > 1$ are bracketed between the values for uniform wall temperature and uniform wall heat flux. However, Figure 4 has indicated that the N_{Nu_h} distributions for $N_L > 1$ display upstream minima, thereby suggesting that in some portion

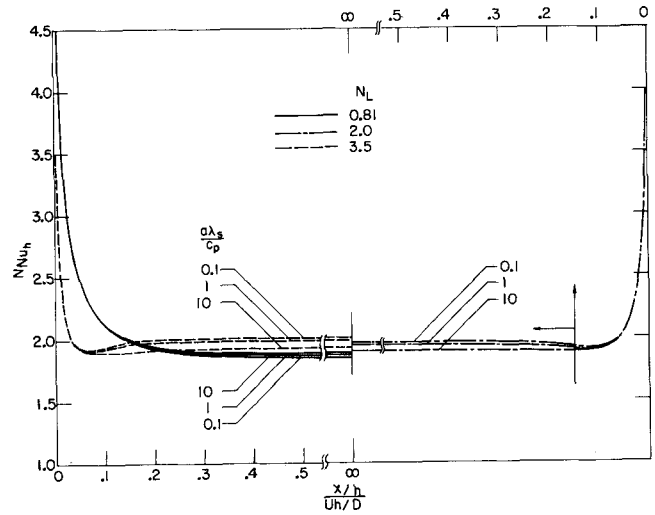

Fig. 4. Nusselt number distributions.

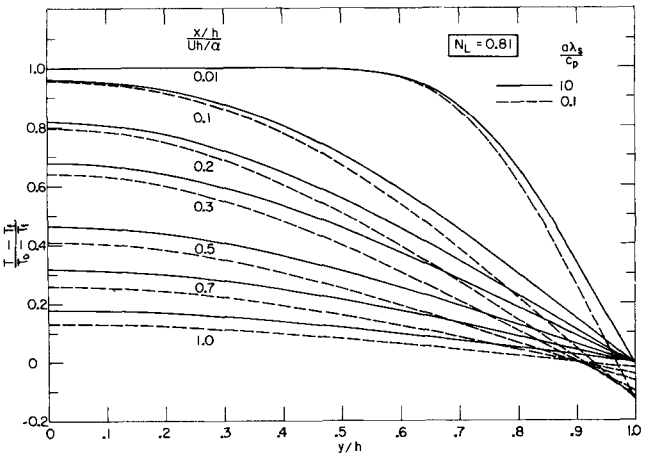

Fig. 5. Temperature profiles, $N_L = 0.81$.

of the entrance region, these curves lie below the N_{Nu_h} curve for uniform wall temperature. These findings confirm that the Nusselt number results for the standard cases of uniform wall temperature and uniform wall heat flux are not necessarily universal bounds.

Temperature and Mass Fraction Profiles

In view of space limitations, only representative temperature profile results can be presented. Figures 5 and 6 have been prepared for this purpose. Each of these figures shows a sequence of temperature profiles corresponding to increasing downstream distances from the entrance section. Figure 5 is for $N_L = 0.81$, while Figure 6 is for $N_L = 3.5$. Results for $a\lambda_s/c_p = 0.1$ and 10 are respectively denoted by dashed and solid lines.

In the immediate neighborhood of the duct inlet, the temperature field is of the boundary layer type, that is, temperature gradients are confined to a layer near the wall and there is an isothermal core. With increasing downstream distance, the effect of the wall heat transfer extends into the core, causing the temperature to decrease. In general, the temperature profiles become flatter with increasing downstream distance, ultimately approaching the fully developed state where $T = T_f$ across the entire cross section.

For $N_L = 0.81$, the temperature profiles are not strongly dependent upon the parameter $a\lambda_s/c_p$. On the other hand, for $N_L = 3.5$, the profiles are quite sensitive to $a\lambda_s/c_p$, with those for smaller $a\lambda_s/c_p$ being flatter.

Mass fraction and temperature profiles are compared in Figures 7 and 8, which correspond respectively to $N_L = 0.81$ and 3.5. All curves in these figures are for $a\lambda_s/c_p = 0.1$. For $N_L = 0.81$, the corresponding mass fraction and temperature profiles are quite similar to each other. This is to be expected, since the heat and mass transfer processes are fully analogous when $N_L = 1$. On the other hand, marked differences between the temperature and

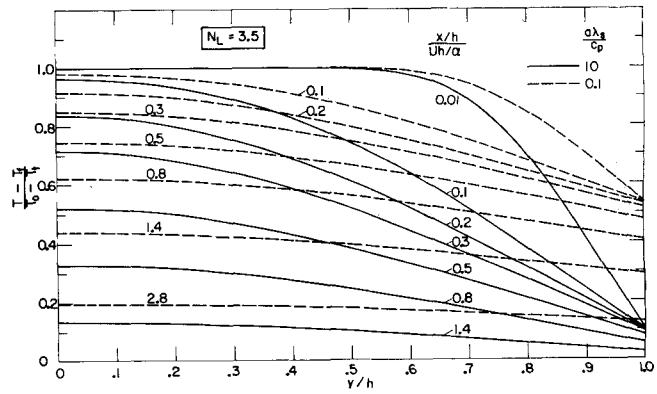

Fig. 6. Temperature profiles, $N_L = 3.5$.

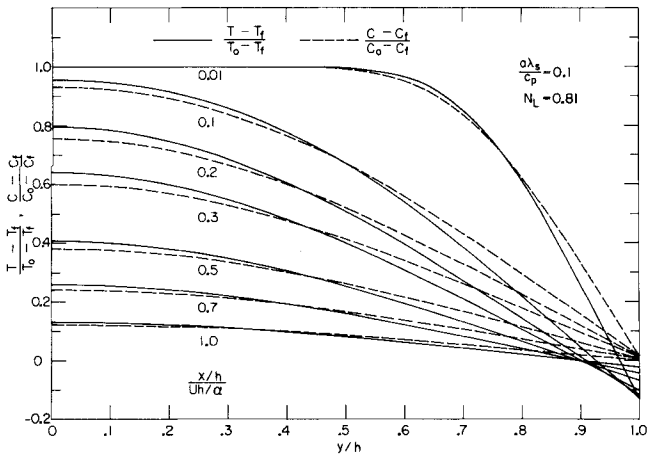

Fig. 7. Comparison between mass fraction and temperature profiles, $N_L = 0.81$.

mass fraction profiles are in evidence when $N_L = 3.5$, indicating a marked departure from the analogy between heat and mass transfer.

Comparison Between Parabolic and Slug Flow Results

A comparison of the entrance lengths corresponding to the parabolic velocity profile with those for the slug flow profile has already been made in Table 1. A more detailed comparison of the developmental characteristics of the two types of flows will now be performed. To this end, Figures 9 and 10 have been prepared to show, respectively, the longitudinal development of the bulk temperature and mass fraction and of the wall temperature. Curves are given for the extreme cases of $N_L = 0.81$ and 3.5, for $a\lambda_s/c_p = 0.1$ and 10. Inspection of the figures shows that the qualitative behavior of the parabolic flow results is faithfully reproduced by the slug flow results. This characteristic is generally assumed to be valid, but frequently without substantiation such as that provided by Figures 9 and 10.

Significant quantitative differences between the two sets of results are brought about by the more rapid longitudinal development that takes place within the slug flow. For quantitative purposes, it is evident that the slug flow results are not a very close approximation of the parabolic flow results.

LÉVÊQUE-TYPE SOLUTION NEAR THE INLET

In the immediate neighborhood of the inlet, the heat and mass transfer processes are confined to thin layers adjacent to the duct walls. The boundary layer developing along one wall of the duct does not interact with the

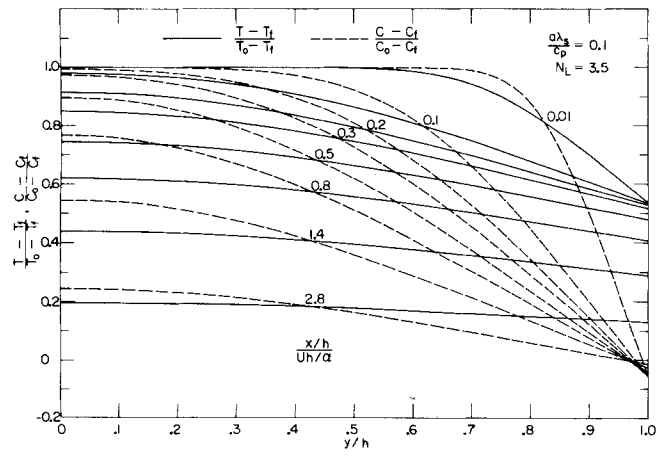

Fig. 8. Comparison between mass fraction and temperature profiles, $N_L = 3.5$.

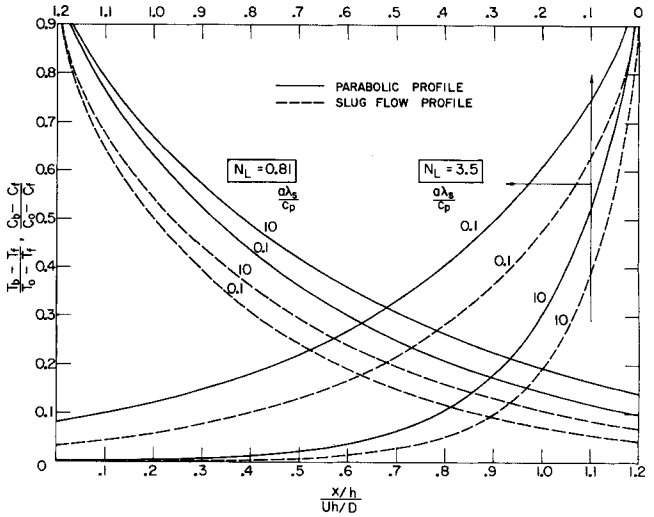

Fig. 9. Comparison of bulk temperature results for parabolic and slug-flow profiles.

boundary layer developing along the opposite wall. In the core of the flow, the temperature and mass fraction are uniform (T_o and C_o respectively). Under these conditions, an approximate solution can be obtained by generalizing a method originally used by Lévêque (7) for the thermal development (without mass transfer) in a circular tube.

Focusing attention on either one of the boundary layers, one approximates the velocity distribution by the expression

$$u/U = 3Y/h \tag{27}$$

where Y is the distance from the wall. Equation (27) represents a straight line which coincides with the tangent to the parabolic profile at the wall. Upon replacing the parabolic velocity profile of Equations (1) with Equation (27) and letting $\zeta = (Y/h)/\xi^{1/3}$, there is obtained

$$-\zeta^2 \frac{d\theta}{d\zeta} = \frac{d^2\theta}{d\zeta^2}, \quad -\zeta^2 \frac{d\phi}{d\zeta} = \frac{1}{N_L} \frac{d^2\phi}{d\zeta^2} \tag{28}$$

The boundary conditions at the wall ($\zeta = 0$) are

$$\frac{d\phi}{d\zeta} = N_L \frac{d\theta}{d\zeta}, \quad \phi = -\left(\frac{a\lambda_s}{c_p}\right)\theta \tag{29}$$

while in the free stream outside the boundary layer

$$\theta \to 1, \quad \phi \to 1 \quad \text{as} \quad \zeta \to \infty \tag{30}$$

The solutions for θ and ϕ are readily found to be

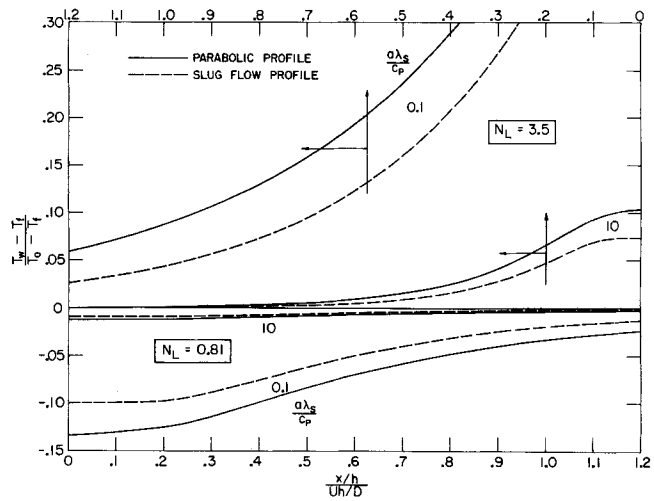

Fig. 10. Comparison of wall temperature results for parabolic and slug-flow profiles.

$$\theta = \left\{ \left(1 + \frac{a\lambda_s}{c_p} \right) F[\zeta/3^{1/3}] + (N_L{}^{2/3} - 1) \right\} \Big/ \left(N_L{}^{2/3} + \frac{a\lambda_s}{c_p} \right) \quad (31)$$

$$\phi = \left\{ N_L{}^{2/3} \left(1 + \frac{a\lambda_s}{c_p} \right) F[\zeta(N_L/3)^{1/3}] + (a\lambda_s/c_p)(1 - N_L{}^{2/3}) \right\} \Big/ \left(N_L{}^{2/3} + \frac{a\lambda_s}{c_p} \right) \quad (32)$$

where

$$F(\Omega) = \frac{3}{\Gamma\left(\frac{1}{3}\right)} \int_o^\Omega e^{-\beta^3} d\beta, \quad F(\infty) = 1 \quad (33)$$

and Γ is the gamma function. At the wall, $\zeta = 0$, the foregoing reduce to

$$\frac{T_w - T_f}{T_o - T_f} = \frac{N_L{}^{2/3} - 1}{N_L{}^{2/3} + (a\lambda_s/c_p)},$$

$$\frac{C_w - C_f}{C_o - C_f} = \left(\frac{a\lambda_s}{c_p} \right) \frac{1 - N_L{}^{2/3}}{N_L{}^{2/3} + (a\lambda_s/c_p)} \quad (34)$$

The wall temperature results provided by Equation (34) will now be compared with those of the series solution derived in the earlier portion of this paper.# The comparison is shown in Table 2. The results from the series solution correspond to $(x/h)/(Uh/\alpha) = 0.005$ which, relative to the abscissa scales of Figures 1 through 4, is very close to the inlet cross section. The results from the Lévêque-type solution are independent of x [Equation (34)].

TABLE 2. COMPARISON OF WALL TEMPERATURE RESULTS FROM SERIES AND LÉVÊQUE-TYPE SOLUTIONS

		$(T_w - T_f)/(T_o - T_f)$	
N_L	$a\lambda_s/c_p$	Series*	Lévêque-type
0.81	0.1	−0.1338	−0.1353
0.81	1.0	−0.06939	−0.07013
0.81	10.0	−0.01194	−0.01206
2.0	0.1	0.3455	0.3481
2.0	1.0	0.2251	0.2270
2.0	10.0	0.05016	0.05069
3.5	0.1	0.5395	0.5427
3.5	1.0	0.3920	0.3949
3.5	10.0	0.1049	0.1061

* Results corresponding to $\xi = (x/h)/(Uh/\alpha) = 0.005$.

Table 2 reveals a deviation of about 1% between the two sets of results. This is ascribed to the approximate nature of the straight line velocity profile expressed by Equation (27). It may be concluded that the utility of the Lévêque type of solution is restricted to the immediate neighborhood of the entrance cross section, where the boundary layer thickness is sufficiently small so that the velocity distribution within the layer is accurately represented by Equation (27).

ACKNOWLEDGMENT

The work of T. S. Chen was supported, in part, by a Summer Research Fellowship for 1967 from the University of Missouri at Rolla.

In view of the second of Equations (29), a comparison of wall temperatures is also equivalent to a comparison of wall mass fractions.

NOTATION

A, B = series coefficients, Equations (19) and (14)
a, b = constants, Equation (7)
C = mass fraction of vapor
c_p = specific heat, constant pressure
D = binary diffusion coefficient
h = channel half height
k = thermal conductivity
N_L = Lewis number, α/D
$\dot{M}$ = axial flow rate
$\dot{m}$ = local sublimation rate/area
N_{Nuh} = Nusselt number, Equation (24)
q = local heat flux/time-area
T = temperature
u = axial velocity
U = average velocity
x = axial coordinate
Y = transverse distance from wall
y = transverse distance from centerline

Greek Letters

α = thermal diffusivity
β = eigenvalue
ζ = coordinate, $(Y/h)/\xi^{1/3}$
η = coordinate, y/h
Θ = function of η
θ = dimensionless temperature, Equation (2)
λ_s = latent heat of sublimation
ξ = coordinate, $(x/h)/(Uh/\alpha)$
ρ = density
Φ = function of η
ϕ = dimensionless mass fraction, Equation (2)

Subscripts

b = bulk
f = fully developed
o = entrance section
w = wall

LITERATURE CITED

1. Kays, W. M., "Convective Heat and Mass Transfer," McGraw-Hill, New York (1966).
2. Hsu, C. J., *AIChE J.*, **11**, 938 (1965).
3. Ulrichson, D. L., and P. A. Schmitz, *IEC Fundamentals*, **4**, 2 (1965).
4. Sparrow, E. M., and E. C. Spalding, *J. Heat Transfer*, **90**, 115 (1968).
5. Hartnett, J. P., and E. R. G. Eckert, in "Recent Advances in Heat and Mass Transfer," J. P. Hartnett, ed., McGraw-Hill, New York (1961).
6. Sherwood, T. K., and R. L. Pigford, "Absorption and Extraction," McGraw-Hill, New York (1952).
7. Boelter, L. M. K., et al., "Heat Transfer Notes," McGraw-Hill, New York (1965).

Manuscript received December 13, 1967; revision received April 15, 1968; paper accepted April 17, 1968.

APPENDIX

Longitudinal Variation in Mass Flow Rate

Let $\dot{M}_o$ and $\dot{M}_f$ represent the mass flow rates at the entrance section and in the fully developed region. Since the flow rate of the non-subliming component must be unchanging, it follows that

$$(1 - C_o)\dot{M}_o = (1 - C_f)\dot{M}_f \quad (35)$$

or

$$\Delta\dot{M} = \dot{M}_f - \dot{M}_o = \dot{M}_o \left[\frac{C_f - C_o}{1 - C_f} \right] \quad (36)$$

Calculations performed in reference 4 suggest that the bracketed factor in Equation (36) will usually be on the order of 1% for flow systems such as air-water and air-naphthalene.